

# The effect of delaminations on local buckling in wind turbine blades



P.U. Haselbach\*, R.D. Bitsche, K. Branner

Technical University of Denmark, Department of Wind Energy, Frederiksborgvej 399, 4000 Roskilde, Denmark

## ARTICLE INFO

### Article history:

Received 27 August 2014

Received in revised form

28 May 2015

Accepted 21 June 2015

Available online xxx

### Keywords:

Buckling

Cohesive elements

Crack growth

Delamination

Nonlinear finite element analysis

Wind turbine rotor blade

## ABSTRACT

In this article the effect of delaminations on the load carrying capacity of a large wind turbine blade is studied numerically. For this purpose an 8.65 m long blade section with different initial delaminations in the main spar was subjected to a flapwise dominated bending moment. The model was setup in Abaqus and cohesive elements were chosen for modelling delamination growth.

For initial delaminations with a width of 30–50% of the cap width the study showed that delamination close to the surface started to grow in load ranges of normal operation conditions and led to local buckling modes. The local buckling caused high strains and stresses in the surrounding of the delamination, which exceeded the material design properties and therefore should be considered as dangerous.

Delaminations placed near the mid-surface of the cap did not have a significant effect on the blade response under normal operation conditions. In the simulations the static load exceeded the design load by more than 40% before delamination growth or cap buckling occurred.

It could be concluded that delamination induced near-surface buckling modes have to be considered critical due to an onset of local sublaminar buckling below the design load level.

© 2015 Elsevier Ltd. All rights reserved.

## 1. Introduction

Areas of poor or no bonding in the interface between adjacent layers of a composite material are defined as delaminations. These interlaminar gaps/cracks normally originate from manufacturing flaws, areas with high stress concentrations around structural discontinuities such as holes, notches, ply drops or connections, or from impact damage during production, transport or service [1–3].

Delaminations embody a local separation of the laminated composite structures into sublaminates. The critical buckling load of the sublaminates may be well below the critical buckling load of the original structure. Consequently, the presence of delaminations may lead to a reduction of structural stiffness and strength. Due to this delaminations in laminated composite structures are considered to be the most critical type of damage that composite structures under compression can experience [4–6].

Delaminations in composite structures can trigger different buckling mode shapes, which poses different levels of danger to the structure. Considering buckling on a panel level the buckling

behaviour of the structure with a delamination can be divided into local and global buckling modes (see Fig. 1) as well as into other combinational modes. A local buckling mode shape represents deformations of mainly one sublaminar on one side of the delamination. This local buckling mode will then introduce bending of the buckled sublaminar and reduce its load carrying capacity. Therefore, the other sublaminar will be subjected to higher compressive loading and additionally experience bending caused by the adjacent buckled sublaminar [7]. Higher ply stresses than in a sound structure will therefore occur, the consequence being that a reduced failure load of the composite structure under compression will arise. A significant reduction of the global critical buckling load can occur. The strength and stiffness reduction can be linked to the initial buckling of the structure. Local buckling typically occurs when the delamination is large and close to the surface (thin sublaminar on one side), which allows one part of the structure to buckle locally; whereas the remaining structure (basic laminate/thick sublaminar) does not buckle. For smaller delaminations located closer to the mid-surface global buckling predominantly occurs, wherein both sublaminars buckle towards the same side.

Under operation conditions wind turbine blades experience high aerodynamic loads, which lead to blade bending. The loading introduces compression on the suction side and tension on the pressure side of blades in normal operation. The loading-carrying

\* Corresponding author.

E-mail addresses: [phih@dtu.dk](mailto:phih@dtu.dk) (P.U. Haselbach), [robi@dtu.dk](mailto:robi@dtu.dk) (R.D. Bitsche), [kibr@dtu.dk](mailto:kibr@dtu.dk) (K. Branner).

URL: <http://www.vindenergi.dtu.dk/>

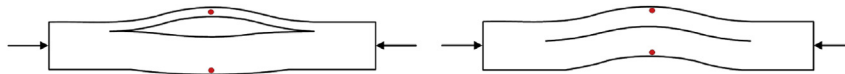


**Fig. 1.** Left: Local buckling mode (local cap opening); Right: Global buckling mode (full cap buckling); figure from Ref. [22]. The red dots symbolise displacement evaluation points. (For interpretation of the references to colour in this figure legend, the reader is referred to the web version of this article.)

structure providing the blade with sufficient strength and stiffness often consists of a main spar and shear webs integrated into the aerodynamic shell. Usually the main spar is made of fibre composite materials, where most of the fibres are oriented in longitudinal direction. Often glass fibres or glass and carbon fibre combinations embedded in epoxy resin matrices are used, providing the composite structure with a high strength-to-weight ratio.

Delaminations may be found within the main spar of the blade. Overgaard et al. [8,9] e.g. investigated experimentally and numerically the structural collapse of a wind turbine blade and came to the conclusion that the structural collapse was caused by multiple local buckling-driven delamination processes. For an accurate assessment of detected delaminations based on size and location in wind turbine blades, guidelines and recommendations are needed.

In order to understand the effect of delamination under compression on laminated composite materials several tests and studies have been conducted. Short et al. [7] tested small glass-fibre-reinforced plastic test specimens, ran Finite Element simulations and developed simple closed-form models for isotropic materials. They also created for flat and curved test specimens a delamination induced buckling mode map for varying delamination sizes and through thickness positions differentiating between local and global.

Studies on the behaviour of delaminations in rectangular composite panels with an initial delamination under compressive loading were carried out by Branner and Berring [10]. They compared experimental findings with a numerical parameter study. Branner and Berring created a buckling mode map for panels under in-plane compression similar to the load carrying flange in the main spar of a typical wind turbine blade. The study showed how the buckling mode shape depends on the size and on the location of the delamination through thickness.

Gaotti et al. [11] studied numerically the panel behaviour under uni-axial loading. They compared advanced numerical prediction methods with the simple models, where delaminations were modelled as disconnected finite element regions.

In all these studies the authors concluded that the panels under uni-axial in-plane loading experience a significantly reduced compressive strength in case of simply supported boundary conditions. Short et al. [7] also concluded that delaminations near the convex side lead to more significant strength reductions than

delaminations near the concave side of the panel. Much work was done to address delaminations on component and panel level. However, due to the assumed boundary conditions used in the studies the authors were limited in drawing solid conclusions whether or not their results can be transferred to full scale wind turbine blade structures. Does a delamination in a main spar of a blade cause a similar strength reduction or does the surrounded structure compensate the local stiffness and strength loss up to a certain size of the delamination? A design criterion for how large and deep delaminations can be accepted without increasing the risk of blade collapse taking the surrounding structure into account is missing.

Such a criterion could help blade manufactures and turbine operators to decide whether a detected delamination can be accepted, needs to be repaired, or whether the blade must be scrapped.

The aim of this numerical study was to investigate how much the strength of a wind turbine rotor blade is affected by delaminations. Two different approaches were used to study the effect of delaminations, where one of the numerical approaches allowed interlaminar crack growth in order to achieve higher accuracy.

## 2. Methods

### 2.1. Modelling method

The DTU 10 MW reference wind turbine blade was used as a basis for simulating the effect of delaminations. The blade, described in detail in Refs. [13], has a length of 86.4 m and a root diameter of 5.4 m. The load carrying structure of the blade is based on two caps and two shear webs. For the studies an 8.65 m long section of the blade was used to investigate delamination behaviour under static load. The section represented the rotor blade in a distance from 41.65 m to 50.3 m from the root at radial position from 44.45 m to 53.1 m (see Fig. 2).

The blade section was modelled with four node shell elements (Abaqus element type S4) in the commercial finite element software Abaqus/CAE 6.12-2. The outer surface of the blade was used as the reference surface containing the finite element nodes (“node offset option”) (see Fig. 3). Apparent material properties were assumed to represent the multi-directional plies instead of a more

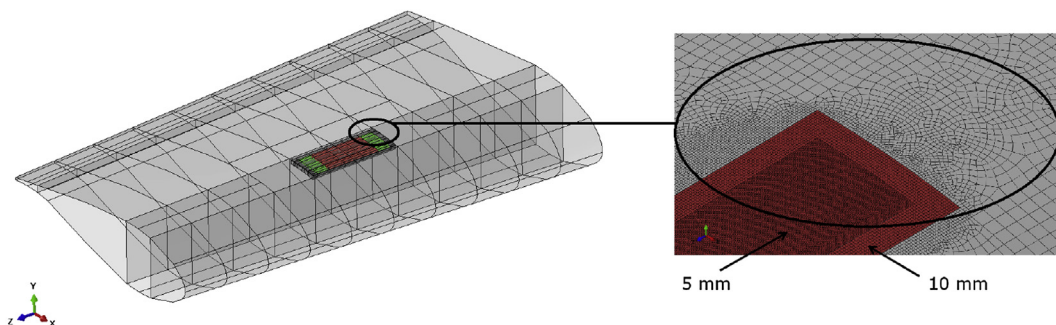


**Fig. 2.** Blade section shell model (grey) of the DTU 10MW Reference Wind Turbine including submodel (red). The submodel on the left picture is subdivided into two section cohesive zone I (red) and cohesive zone II (green). (For interpretation of the references to colour in this figure legend, the reader is referred to the web version of this article.)

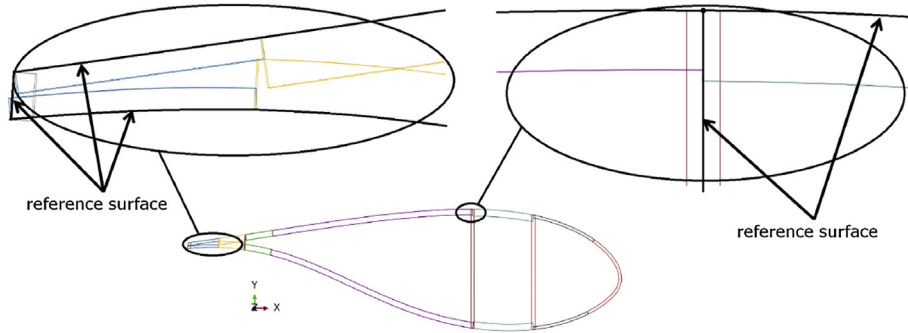


Fig. 3. Simplifications due to the shell modelling approach.

detailed lay-up description. The entire layup and the material properties for the blade are available online: <http://dtu-10mw-rwt.vindenergi.dtu.dk/> and can be accessed after free registration. In this paper only the apparent material properties of the unidirectional material used in the caps is given in Table 1 to illustrate the properties of the region studied in detail. The critical energy release rate values were chosen according to typical magnitudes for unidirectional composite materials [14].

Further simplifications were made due to the shell modelling approach. The trailing edge and the cap/web joints were modelled in a general way without specifying the geometrical details at the joints. The modelling strategy is shown in Fig. 3 for the shear web to cap joints and the trailing edge joint, where simple edge to edge joints were assumed.

The shell model contains 60,999 four node shell elements. The typical elements in the model had a characteristic element length of 0.05 m. Mesh refinement applied to shell elements around the area of interest, where an initial delamination was modelled, reduced the characteristic element length to 0.01 m.

The region surrounding the delamination was discretised using a fine mesh of solid brick elements. In the following this region will be referred to as “submodel”. The term should not be confuse with a technique of the same name, where a local part of a model is analysed based on interpolation of the solution from a coarser mesh. In our simulation the submodel was implemented in order to simulate buckling driven delamination growth in the cap. The submodel had a span of ca. 1.7 m and was placed centrally in the cap (see Fig. 2). The width of the cap (B) varied between 0.707 m and 0.725 m. The thickness of the cap at this location was 0.0817 m.

In order to investigate the behaviour of rotor blades with initial delaminations, rectangularly shaped delaminated areas were centrally positioned in the submodel. The initial delaminated areas varied in size and position through the thickness. The ratio  $t/T$  described the position through the thickness (see Fig. 4) with the total cap thickness  $T = 0.0817$  m and the distance to the outer

surface  $t$ . The length ( $a$ ) and width ( $b$ ) of the initially delaminated area were varied. For all simulations in this study the aspect ratio  $a/b = 1.29$  was used. This aspect ratio was chosen to promote the formation of a single buckle at low loads. The minimum buckling load (critical buckling load =  $N_0$ ) depends on both the elastic properties and the initial delamination size ( $a, b$ ) and position ( $t$ ).

For the cap with the material properties given in Table 1 the aspect ratio  $a/b = 1.29$  can be derived for orthotropic panels subjected to uniaxial in-plane compression where all edges are simply supported [1,10,11]. The assumption leads to the following equation:

$$N_0(m, n) = \pi^2 \left[ D_{11} \left[ \frac{m}{a} \right]^2 + 2(D_{12} + 2D_{66}) \left[ \frac{n}{b} \right]^2 + D_{22} \left[ \frac{n}{b} \right]^4 \left[ \frac{a}{m} \right]^2 \right] \quad (1)$$

where  $N_0$  is the critical buckling load in terms of a force per length,  $D_{ij}$  are the elements of the bending-stiffness matrix from classical laminate theory which relates bending and torsion moments with curvatures, and  $m$  and  $n$  are the numbers of buckle half wavelength in spanwise and transverse direction, respectively. Assuming  $n = 1$  it can easily be shown that the critical buckling load  $N_0$  is minimal if:

$$m = \frac{a}{b} \left[ \frac{D_{22}}{D_{11}} \right]^{\frac{1}{4}} \quad (2)$$

Assuming  $m = 1$  in Eq. (2) yields  $a/b = 1.29$ . The aspect ratio is similar to the results Braner et al. presented in Ref. [7] with  $a/b = 1.31$ .

The submodel is a highly discretised 3D model of the cap (see Fig. 2) consisting of incompatible mode eight-node brick elements (Abaqus element type: C3D8I) and 3D cohesive elements (Abaqus element type: COH3D8). The cohesive elements were placed in a  $0.817 \text{ mm} (=1/100 \cdot T)$  thin layer. The cohesive elements provided the possibility of delamination growth whereas the initial delamination was modelled by a missing layer of elements corresponding to the size of the delaminated area. Contact constraints are used to prevent element interpenetration.

The submodel has two different mesh densities with an element length of 0.01 m and 0.005 m, respectively, in order to smoothen the transition between the coarser shell and the finer brick elements (see Fig. 2). The entire submodel consists of approximately 180,000 solid elements and 22,000 cohesive elements. The solid elements are equally distributed into seven layers through the thickness. The outer (rougher) and inner (finer) submodel element areas were tied together via so-called tie constraints (provided by Abaqus).

The submodel 3D brick elements were coupled with suitable constraint equations to the shell element edges of the basic model (shell-to-solid coupling provided by Abaqus).

Table 1

Apparent material properties of the unidirectional composite material. Young's modulus ( $E$ ), Poisson's ratio ( $\nu$ ), density ( $\rho$ ), shear modulus ( $G$ ), critical energy release rate ( $G_c$ ), mixed mode exponent ( $\eta$ ), maximum traction ( $\tau$ ), stiffness of the interface ( $K$ ), critical strain parameter ( $\epsilon$ ), safety factor ( $\gamma$ ) [13–15].

$E_{11}$	$E_{22}$	$E_{33}$	$\nu_{12}$	$\nu_{13}$	$\eta$
41.63 GPa	14.93 GPa	13.43 GPa	0.2410	0.2675	3.8
$\nu_{23}$	$\rho$	$G_{12}$	$G_{13}$	$G_{23}$	
0.3301	1900 kg/m <sup>3</sup>	5.047 GPa	5.047 GPa	5.047 GPa	
$G_{Ic}$	$G_{IIc}$	$G_{IIIc}$	$\gamma_F$	$\gamma_{Ma}$	
200 J/m <sup>2</sup>	1000 J/m <sup>2</sup>	1000 J/m <sup>2</sup>	2.205	1.35	
$\tau_I$	$\tau_{II}$	$\tau_{III}$	$\epsilon_I^T$	$\epsilon_I^C$	
7.5 MPa	15 MPa	15 MPa	2.10%	1.50%	
$K_{mm}$	$K_{ss}$	$K_{tt}$	$\epsilon_I^T/\gamma_{Ma}$	$\epsilon_I^C/\gamma_{Ma}$	
3e14 N/m <sup>3</sup>	1.15e14 N/m <sup>3</sup>	1.15e14 N/m <sup>3</sup>	0.9523%	0.6802%	

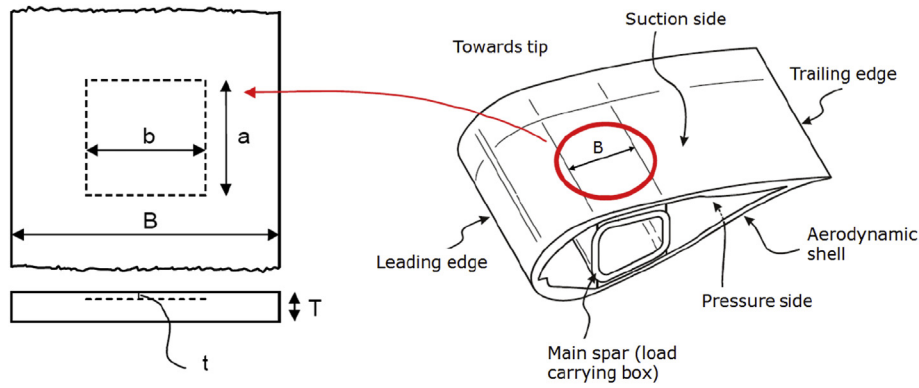


Fig. 4. Geometrical description of positioning the initial delaminated [12].

### 2.1.1. Cohesive elements

Cohesive elements were chosen for modelling delamination growth because this method allows existing cracks to grow and also to initiate new cracks within the framework of Continuum Damage Mechanics (CDM) [15].

In general material damage considers crack initiation, crack growth and crack merging. CDM describes the state of damage with a damage variable ( $d$ ). The variable ranges between  $d = 0$  (no damage) and  $d = 1$  (full damage). The material fails completely when the value  $d = 1$  is reached. CDM can be described with the cohesive zone model (CZM) approach. Within the energy based CZM approach material properties, crack initiation conditions and a crack evolution functions are defined and can be visualised in a tension softening diagram.

A critical energy release rate defines the area under the traction-separation-relation. Cohesive elements are used to model material discontinuities and damage based on Griffiths energy approach [16,17]. For the current work a bilinear traction-separation relation was chosen because of its simplicity [17].

The energy release rate associated with delamination growth strongly depends on the fracture mode. The criteria for crack initiation and crack propagation have to take mode-mixity into account. Generally, three different modes of fractures are assumed and consequently also three traction-separations laws according to the different interfacial strength and maximum tractions have to be defined. The delamination growth process starts when the stresses and/or strains satisfy a damage initiation criterion. In the present work a quadratic nominal stress criterion was used to interpolate between these different traction-separation laws. The criterion assumes damage initiation when a quadratic interaction function reaches the value one (see Fig. 5).

The delamination evolution was defined by the Benzeggagh-Kenane (BK) fracture criterion [18], which considers the dependence of the fracture energy on the mode mixity. The BK criterion is particularly useful when the critical fracture energies for the second and third mode of fracture are the same, which is commonly assumed.

The BK fracture criterion is defined by the components of the energy release rate  $G_i$  and the critical energy release rate  $G_i^c$  (see Fig. 5). Further assumptions were that the delamination can only propagate in the interface between two plies. The interface was represented by the cohesive elements. Additionally, the delamination cannot jump between the plies during crack propagation because the model only contains one layer of cohesive elements [15,19].

In numerical FEM analyses the calculation time is mainly determined by the number of degrees of freedom (DOF) of a model.

Therefore, on the one hand the mesh discretisation should be as coarse as possible. On the other hand often fine discretizations are needed to yield accurate results. Especially in areas, where stress concentrations are expected or energies have to be determined accurately. The latter is the case for the process zone of the cohesive layer where the crack propagation takes place. The length of the process zone is called cohesive zone length ( $l_{cz}$ ). The cohesive zone length should contain at least three elements to calculate the energy release rate during the delamination growth precisely [20]. The length of the process zone can be estimated as: (Hillerborg's model) [20]

$$l_{cz} = M * E * \frac{G_c}{(\bar{\tau}^0)^2} \quad \text{with } M = 1 \quad (3)$$

where  $M$  is a parameter depending on the adopted calculation model. The interfacial strength is expressed by  $\bar{\tau}^0$ ,  $G_c$  is the critical energy rate and  $E$  the Youngs modulus.

Typically, glass fibre epoxy or carbon fibre epoxy composite materials have a  $l_{cz}$  that is only a few millimetres long. Discretisation of the  $l_{cz}$  with at least three elements would require an element size of around a millimeter or smaller depending on the material. The calculation time to analyse large structures with such a high discretisation would cause problems and predictions for large scaled progressive delaminations would not be realised in reasonable time with current state of computational power.

An engineering solution for using coarser meshes was given by Turon et al. [16] by artificially lowering the interfacial strength. Lowering the interfacial strength ( $\bar{\tau}^0$ ) increases the  $l_{cz}$ . As a consequence the length of each element ( $L_e$ ) in the cohesive zone can be increased, which decreases the calculation time without having a strong influence on the accuracy:

$$N_e = \frac{l_{cz}}{L_e} \quad (4)$$

According to Turon et al. [16] the required  $\bar{\tau}^0$  for a desired  $L_e$  and  $N_e$  representing the  $l_{cz}$  can be calculated by

$$\bar{\tau}^0 = \sqrt{\frac{9 * \pi * E * G_c}{32 * N_e * L_e}} \quad (5)$$

The reduction of  $\bar{\tau}^0$  by e.g. a factor of 10 increases the length of the cohesive zone by a factor 100. Table 1 shows the used material properties, where  $\bar{\tau}^0$  was reduced by a factor of seven compared to a typical interfacial strength of glass fibre epoxy with  $\bar{\tau}^0 = 53$  MPa.

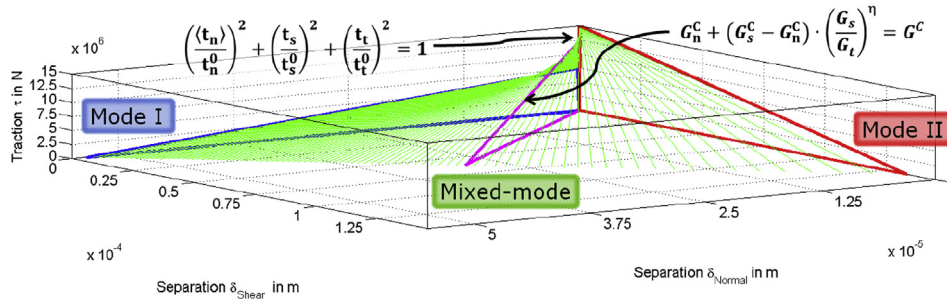


Fig. 5. Illustration of mixed-mode response in cohesive elements with Benzeggagh-Kenane fracture criterion (equation on the right hand side) and quadratic damage initiation interaction function (equation on the left hand side).

In the numerical study the cohesive element layer was divided in two sections (cohesive zone I and cohesive zone II) as shown in Fig. 2. The partition ensured that delamination growth always initiated around the initially delaminated area and avoided artificially induced delamination growth evoked by stress concentrations at the transition zones between the zones with different level of discretisation. Cohesive zone II describes the material properties of the first and last 0.1 m in radial position of the cohesive elements which embody the transition to the coarser solid elements. Cohesive zone I specifies the material properties of the remaining cohesive elements. The critical energy release rate between cohesive zone II were increased by a factor of ten compared to the values for cohesive zone I given in Table 1 in order to ensure delamination growth starting around the initial delaminated area and not at areas with artificially high stresses and strains due to mesh refinement.

2.1.2. Numerical analysis and boundary conditions

In order to simulate delamination growth moments dominated by flapwise bending, comparable to those blade structures experience under normal operation conditions, were applied. All nodes representing the back section (the section closest to the root) were fully constrained. The nodes representing the front section were coupled to a reference node using a so-called kinematic coupling constraint (see Fig. 6). This forces the front section to move like a rigid body. Three moments were applied to the references node at the front section:  $M_x = -16.4e6 \text{ Nm}$ ,  $M_y = 2.4e6 \text{ Nm}$  and  $M_z = 0.32e6 \text{ Nm}$ . The moments correspond to approximately 100% of the moments of the design loads evaluated for the blade cross section at  $r = 48.775 \text{ m}$  (middle of the simulated blade section).

Experimental investigations on the compressive strength of thick composite panels have shown that the loading has to be high before delaminations located close to the centre of the panels propagate [10]. In order to ensure delamination growth for all simulated cases, the applied moment was scaled up to 200% of the design load including the safety factor of 1.35. 100% of the load applied to the sound blade section leads to maximum and

minimum strain values of around 0.6% at a load level of 100% of the design load. At a load level between 125% (compression) to 145% (tension) the design strain values (see Table 1) are reached.

The numerical study is based on a quasi-static nonlinear analysis implemented in Abaqus/Explicit. The Abaqus/Explicit solver employs an explicit time integration scheme [21]. The explicit solver was chosen due to its efficiency when analysing large models and because it is really suited for models which exhibit a softening response (cohesive elements), and contact. No mass scaling was used. In order to simulate a quasi-static loading process the loading speed was kept so low that the kinematic energy of the system was very small compared to the internal energy of the structure ensuring that inertia forces were insignificant.

Two different modelling approaches were conducted. One approach only included solid elements in the submodel, but no cohesive elements, and therefore did not allow delamination growth. This approach is referred to as "solid element approach" in the following.

Cohesive elements were used for the second modelling strategy. This approach allowed delamination growth around the initial delamination. The delamination growth was limited to the area of the cohesive elements. The approach is referred to as the "cohesive element approach" in the following.

Three different initial delamination sizes (variation of  $b/B$ ) placed at different thicknesses ( $t/T$ ) in the laminate were studied. The width took the values  $b/B = 0.278$ ,  $b/B = 0.4$  and  $b/B = 0.5$ . The delaminations were placed in thicknesses of  $t/T = 0.05$  up to  $t/T = 0.35$ , divided in steps of  $\Delta t/T = 0.05$ .

3. Results

A shell model including the implemented submodel without delamination was validated against the original blade shell model without submodel. No significant differences between both models were found. Also the stresses and strains at the interface from the shell to solid elements showed smooth transition. The submodel approach has therefore been found reliable and suitable.

The local occurring buckling modes in the main spar were divided into two different groups *full cap buckling* and *local-cap opening*. The out-of-plane displacement of the central nodes of the sublaminates (see Fig. 1) were used to distinguish between the local cap opening and full cap buckling. The full cap buckling is comparable to global buckling on panel level. It is characterized by both nodes following the same path [22]. The sublaminates on both sides of the delamination move in the same out-of-plane direction, which usually leads to delamination gap closing. The local cap opening buckling mode is comparable to local buckling on panel level. The central nodes of the sublaminates move in opposite out-of-plane directions and cause an opening of the delamination [22].

Furthermore stable and unstable delamination growth was

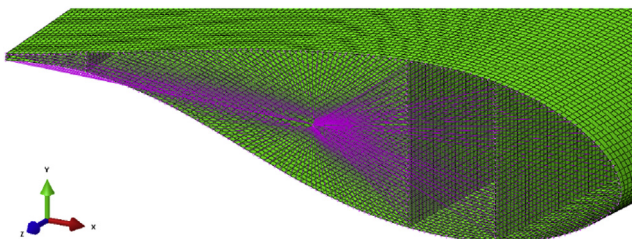


Fig. 6. Boundary condition at the front end of the blade section.

observed. For delaminations close to the surface stable delamination growth was observed. Stable delamination growth is characterised by gradual crack propagation and a slow increase of dissipated energy, respectively. Increasing loading is required in order to have crack propagation under stable crack growth conditions. Unstable/sudden delamination growth is characterized by progressive crack propagation without or with only very little additional loading. The delamination grows significantly faster and partly independent from additional external energy. Unstable delamination growth occurred for delaminations located deeper inside the caps.

### 3.1. Local cap opening buckling mode with stable crack growth

For local cap opening modes with stable delamination growth the solid and the cohesive element approach showed good agreement regarding buckling onset such as the one example shown in Fig. 7(a). At a load level of approximately 50% the upper sublaminates buckled whereas the basic laminate (lower sublaminates) remained undeformed. The delamination led to a local cap opening buckling mode. Simultaneously with the opening of the initial delamination, the delamination started to grow. The delamination propagation originated from the initial delaminated area and grew circularly around it (see Fig. 8(a) to Fig. 9(b)). This phenomenon was indicated by the dissipated energy and the damage stage of the cohesive elements. At a load level of approximately 135% the out-of-plane displacement of the upper sublaminates (cohesive element approach) shows a small kink. This kink can be explained with changes in the buckling mode shape. The sine-shaped buckling mode with a single local cap opening buckle was moving towards another buckling mode configuration with three buckles (see Fig. 10).

At low load levels both modelling approaches showed small reductions in the bending stiffness caused by the Brazier effect [23] (see Fig. 7(b)). The bending stiffness was determined by dividing the applied bending moment by the strain at the center of the cap on the pressure side in longitudinal direction. At a load level of approximately 50% buckling occurred and delamination growth started, which caused a progressive decrease of the bending stiffness for the cohesive element approach. No significant changes in the bending stiffness due to the buckling could be observed for the solid element approach at this load level.

The next significant decrease happened at a loading of around 135% for the cohesive element approach. The decrease of the

bending stiffness was accompanied by the change in the buckling mode shape, which showed progressive decrease. A small increase of the bending stiffness due to contact between the upper and lower sublaminates at a load level around 175% occurred. First at load levels of more than 160% the solid element approach showed a progressive decrease in the bending stiffness. However, the blade bending stiffness only slightly decreased in the overall performance with less than 1% for both approaches for loads up to the design load and up to 2% for a load factor of 2.

During the buckling of the sublaminates high stresses and strains in the upper sublaminates occurred. In Fig. 11 the longitudinal normal strain of the blade section with a cap opening buckling mode is plotted at a loading of 80%. The colour bar for the design strain values for the unidirectional material used in the main spar ranges from red (in web version) (tensile design strain,  $\epsilon_1^T/\gamma_{Ma} = 0.9523\%$ ) to blue (in web version) (compressive design strain,  $\epsilon_1^C/\gamma_{Ma} = -0.6802\%$ ). The black colour indicates areas where the compressive design strain value is exceeded. The figure shows that the cap opening buckling mode causes stress concentrations and that the compressive strain around the initial delamination in the upper sublaminates exceeds the compressive strain design value ( $\epsilon_1^C/\gamma_{Ma}$ ) by more than 40%. The local cap opening buckling modes with stable delamination growth caused less than 1% decrease of the bending stiffness at the design load level but caused high strains and stresses in the surrounding of the delamination. This high strains and stresses in the upper sublaminates were close to and partly even above the material design properties and could easily have led to material failure.

For all simulated delaminations that caused local cap opening buckling with stable delamination growth the critical buckling load, when delamination propagation started, was below the maximum design load. The local cap opening buckling modes led to a bending stiffness reduction of less than 1% for loads lower than the design load. The fact that the delamination grew already at these load levels raises awareness of how critical delaminations can be.

### 3.2. Local cap opening buckling with sudden/unstable crack growth

The differences between the simulations based on the solid element approach and simulation based on the cohesive elements approach became apparent for local cap opening buckling modes with sudden/unstable crack growth. The models with cohesive elements showed local cap opening up to a thickness ratio of  $t/$

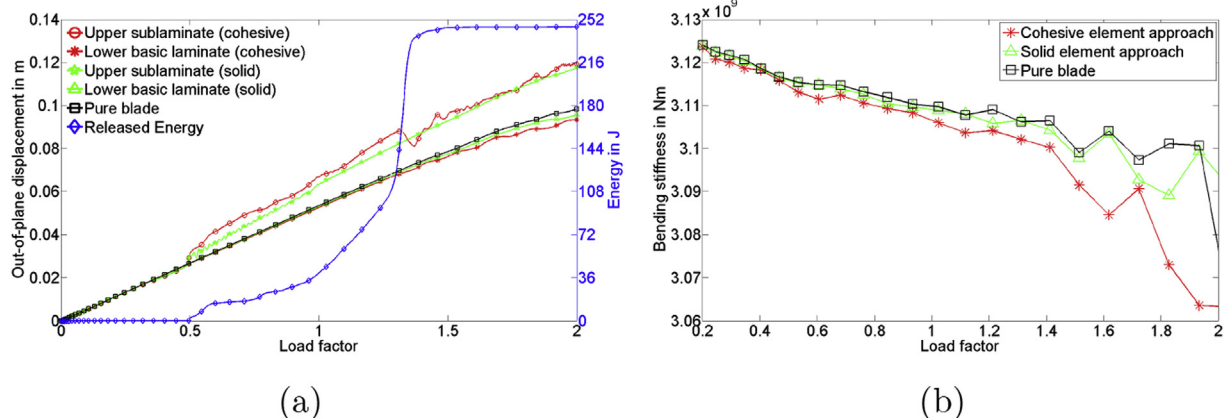


Fig. 7. (a) Local cap opening buckling mode with stable crack growth ( $t/T = 7.5\%$ ,  $b/B = 0.40$ ). The figure shows the out-of-plane displacement of the central points and the released energy as a function of the load. (b) Bending stiffness plot of the entire blade section evaluated at the pressure side in the middle to the cap.

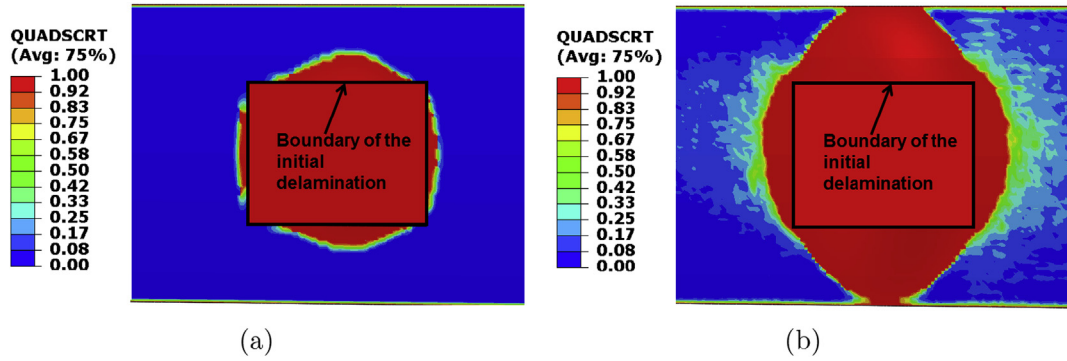


Fig. 8. The figures show the progressive damage initiation of the cohesive elements around the initial delamination (white square) for local cap opening buckling mode with stable crack growth ( $t/T = 7.5\%$ ,  $b/B = 0.40$ ) for different load levels. The variable ranges between  $d = 0$  (no damage) and  $d = 1$  (full damage).

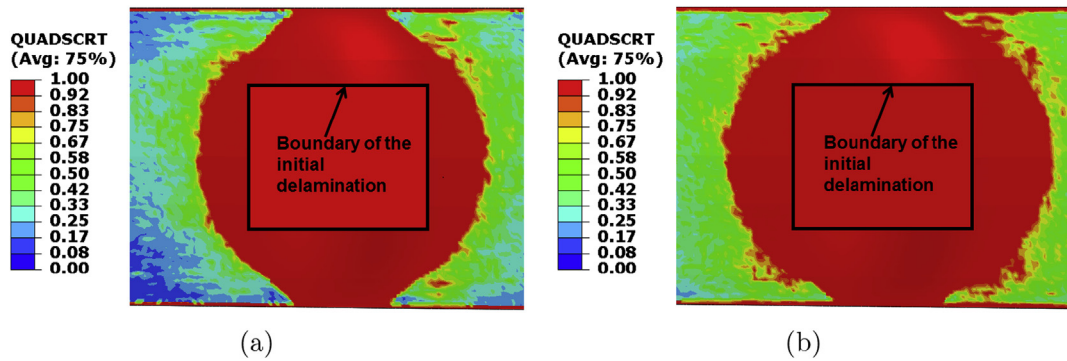


Fig. 9. The figures show the progressive damage initiation of the cohesive elements around the initial delamination (white square) for local cap opening buckling mode with stable crack growth ( $t/T = 7.5\%$ ,  $b/B = 0.40$ ) for different load levels. The variable ranges between  $d = 0$  (no damage) and  $d = 1$  (full damage).

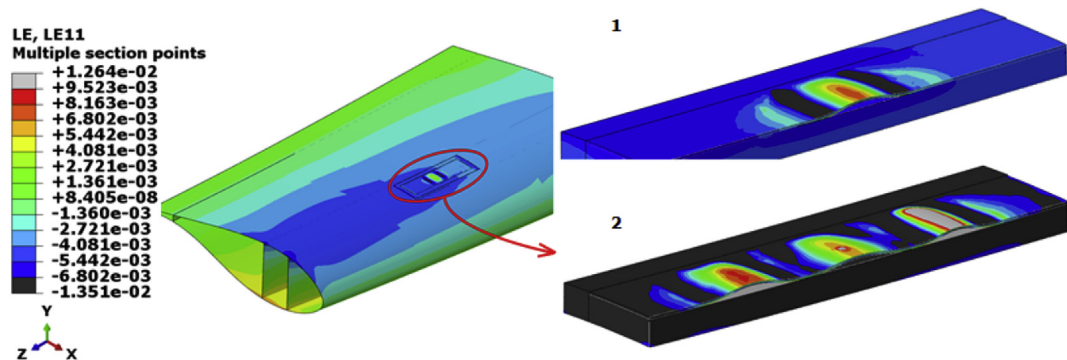


Fig. 10. Local cap opening buckling mode with stable crack growth ( $t/T = 7.5\%$ ,  $b/B = 0.40$ ). The strain in longitudinal direction is plotted. The colour bar indicates the design strain values of the longitudinal tensile strain (0.9523%) and compressive strain ( $-0.6802\%$ ) to failure. The sine-shaped local cap opening buckling mode with a single buckle at 100% loading (Picture 1.) moved towards another buckling mode configuration. Picture 2 represents the buckling mode shape at a load level of 150%.

$T = 0.25$ , whereas models with solid elements had already shown a delamination closing and tended towards full cap buckling behaviour at that thickness ratio (see Fig. 12(a)).

The graphs representing the solid model without delamination growth possibility (solid element approach) showed delamination gap closing/full cap buckling at high loads. The initial delamination size to depth ratio prevented the solid model from local cap opening buckling. While delamination growth for initial delaminations close to the surface (low  $t/T$  ratio) were driven by buckling at low loads and with stable delamination propagation, the opposite was the case for deeper placed initial delaminations. For delaminations deeper inside the main spar, the thicker

sublaminates were less flexible and could withstand higher loads before buckling onset. For simulations based on the cohesive element approach delamination growth occurred due to the high stresses and strains before cap opening buckling occurred. The delamination propagation operated like a splitting of the load carrying main spar and extended the area of the initial delamination. Delamination-driven buckling occurred. For initial delaminations placed at  $t/T \geq 0.15$  the buckling first occurred at load levels significantly above the maximum design load level (>125% loading) and with prior delamination growth as shown in Table 2. Before reaching these high load levels the blade section had already exceeded the design strain values in the main spar as shown on the

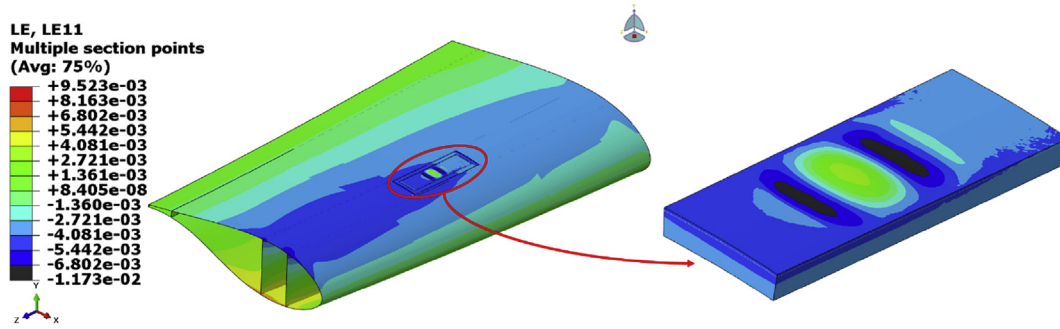


Fig. 11. Local cap opening buckling mode with stable crack growth ( $t/T = 10\%$ ,  $b/B = 0.50$ ). The strain in longitudinal direction under 80% of the design load is plotted. The colour bar indicates the design strain values of the longitudinal tensile strain (0.9523%) and compressive strain (0.6802%) to failure.

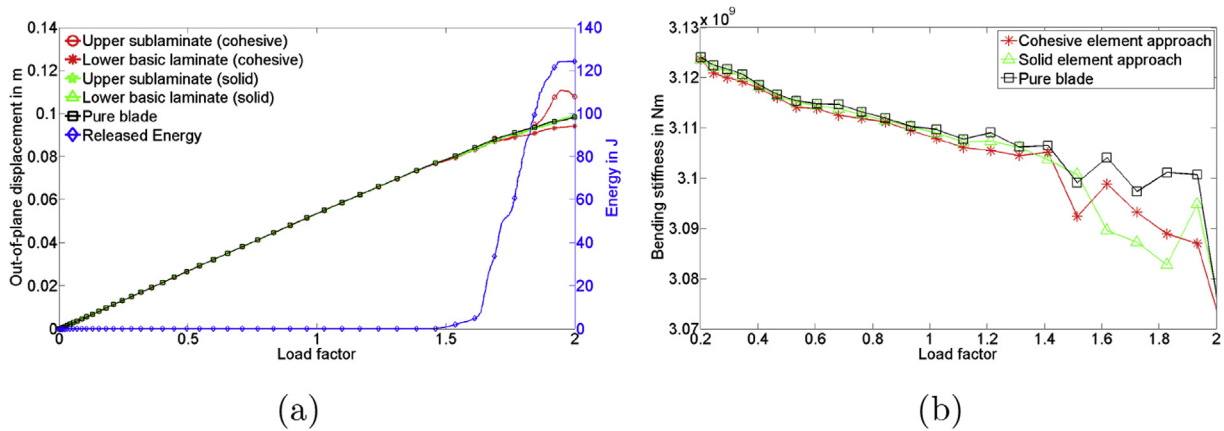


Fig. 12. (a) Local cap opening buckling mode and cap closing buckling mode with sudden/unstable crack growth ( $t/T = 25\%$ ,  $b/B = 0.50$ ). The figure shows the out-of-plane displacement of the central points and the released energy as a function of the load. (b) Bending stiffness plot of the entire blade section evaluated at the pressure side in the middle to the cap. The bending stiffness reduces after passing the design load (load factor = 1).

sound blade structure in Fig. 13.

For the cohesive element approach a clear reduction of the bending stiffness first occurred when the delamination started to grow (see Fig. 12(b)). Before the delamination growth started the reduction of the bending stiffness was mainly caused by the Brazier effect [23]. The cohesive element approach predicted the bending

stiffness degradation at an earlier stage due the delamination growth and thus an increase of the delamination. At a certain load level the delamination started to grow in size and consequently the delaminated area got large enough to cause local cap opening buckling at the given load level. In cases where simulations based on the solid element approach predicted full cap buckling behaviour/delamination closing, it can be concluded that the size of the initial delamination was too small and too deep through the thickness to cause local cap opening. However, the maximum bending stiffness reduction for both approaches was less than 1.5%.

Table 2

Results of the delamination study, width ratio ( $b/B$ ), delamination placed in through cap thickness ratio ( $t/T$ ), local cap opening buckling load ( $P_{open}$ ), buckling mode shape, delamination growth onset as a factor of the design load.

$b/B$	$t/T$	$P_{open}$ coh.	$P_{open}$ solid	Buckling mode	Del. onset
0.278	0.05	0.53	0.54	Local cap opening	0.53
0.278	0.075	1.08	1.11	Local cap opening	1.08
0.278	0.010	1.55	1.59	Local cap opening	1.55
0.278	0.015	1.84	–	Local cap opening	1.60
0.278	0.020	1.90	–	Local cap opening	1.60
0.278	0.025	1.90	–	Local cap opening	1.60
0.278	0.030	–	–	Cap closing	1.60
0.40	0.05	0.24	0.24	Local cap opening	0.34
0.40	0.075	0.50	0.50	Local cap opening	0.50
0.40	0.010	0.80	0.80	Local cap opening	0.80
0.40	0.015	1.50	1.50	Local cap opening	1.42
0.40	0.020	1.64	–	Local cap opening	1.53
0.40	0.025	1.83	–	Local cap opening	1.53
0.40	0.030	–	–	Cap closing	1.53
0.50	0.010	0.60	0.59	Local cap opening	0.60
0.50	0.015	1.26	1.25	Local cap opening	1.25
0.50	0.020	1.53	1.65	Local cap opening	1.38
0.50	0.025	1.75	–	Local cap opening	1.42
0.50	0.030	–	–	Cap closing	1.42

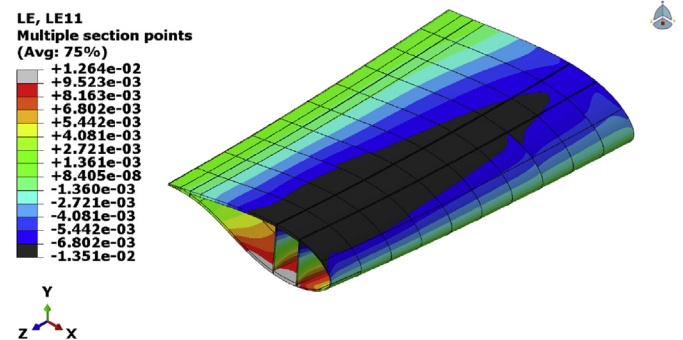


Fig. 13. Strain distribution in the sound blade structure at a load level of around 146% of the designated load.

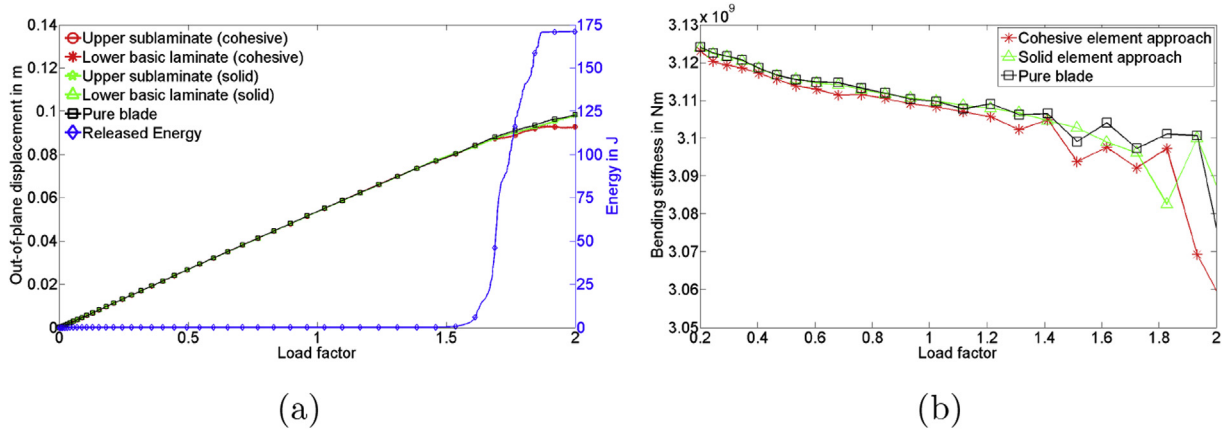


Fig. 14. (a) Full cap opening buckling mode with sudden/unstable delamination growth ( $t/T = 30\%$ ,  $b/B = 0.40$ ). The figure shows the out-of-plane displacement of the central points and the released energy as a function of the load. (b) Bending stiffness plot of the entire blade section evaluated at the pressure side in the middle to the cap.

### 3.3. Full cap buckling

Full cap buckling modes occurred for both simulation approaches when the initial delamination was positioned deep inside the structure. The blade model with cohesive elements showed blade collapse on lower load levels than the model based on the solid element approach due to a significant reduction in the bending stiffness caused by delamination growth. Typical observed full cap buckling behaviour responses looked like the one example shown in Fig. 14(a). In all simulated cases, where full cap buckling had been observed, the load level was higher than 140% of the design load before a significant bending stiffness reduction could be observed. By exceeding this load level high stress and strain levels were also obtained. These high stresses and strains exceeded the design strain values but were still below the critical material strain values when critical buckling loads were reached as shown in Fig. 13. For models based on the cohesive element approach delamination growth always had occurred before full cap buckling occurred. The simulations showed clear differences between both approaches regarding the bending stiffness reduction (see Fig. 14(b)). The cohesive element approach clearly predicted more conservative results with bigger losses in the bending stiffness than the solid element approach. The bending stiffness degradation for the cohesive element approach happened on lower load levels. The extension of the delaminated area during delamination growth process led to the earlier bending stiffness reduction. The alternation of the bending stiffness starting around a load level of 130% resulted from the contact during the gliding between the upper and lower delaminated sublaminates during the buckling process. However, the maximum bending stiffness reduction was less than 1% for loads up to the design load.

All buckling modes that occurred during the study are summarised in Fig. 15 and Table 2. The modes, as described above, were divided into different buckling modes, local cap opening buckling mode and full cap buckling mode. In the figure the buckling modes are plotted with their initial delamination width  $b/B$  over the position through the cap thickness  $t/T$ . For each configuration both modelling approaches were adopted and compared.

### 3.4. Blade vs. panel studies

The buckling mode map (Fig. 15) clearly shows that the bigger the initial delamination was in size the bigger the tendency for local cap opening buckling modes. This tendency is compliant with the observation of panel experiments and simulations conducted by

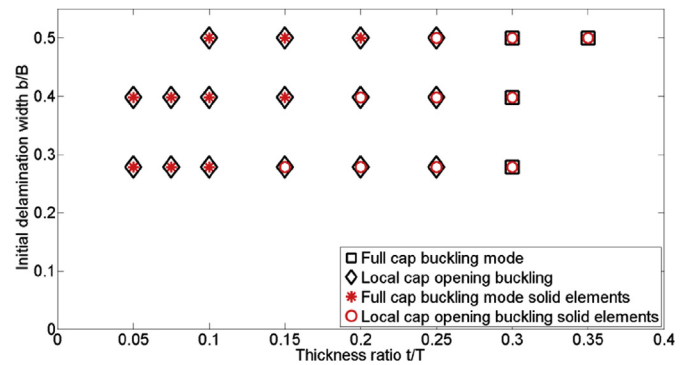


Fig. 15. Buckling mode map for the cap section with an initial delamination aspect ratio  $a/b = 1.29$ .

Branner and Berring [10].

However, differences arose when comparing the Branner and Berring's residual strength map for simply supported composite panels with imbedded delaminations published in Ref. [10] with the results of the current blade study. Branner and Berring's residual strength map shows for delaminations with a size of  $b/B = 0.3$  and a through thickness positioning ratio between  $0 < t/T < 0.5$  no or less than 5% reduction of the compressive strength for the load carrying capacity of the panels. Comparing these results with the present blade study similar results were found if the design load (load factor of 1) is considered to be the maximum load the blade has to withstand.

Looking at delaminations with a size of  $b/B = 0.5$  and a through thickness positioning ratio between  $0 < t/T < 0.5$ , Branner and Berring predicted a compressive strength reduction between 5% and 15% of its load carrying capacity. Only very little reductions of the bending stiffness of less than 1.0% for loads up to the maximum design load (load factor of 1) could be noticed in the blade study.

The delaminations in the main spar of the blade under quasi-static loading did not cause the same bending stiffness reduction as strength reductions observed in the panel experiments and simulations conducted by Branner and Berring [10]. Reflecting the results from the blade study, the results make sense anyway. Considering 60% of the blade flapwise bending stiffness is provided by the caps, each cap provides 30% of the flapwise bending stiffness. If the upper 10% of the bending stiffness over the complete cap width  $B$  would be removed and would not contribute at all to the overall blade bending stiffness, the bending stiffness would be

reduced by maximum 3%.

It seems that differences in boundary conditions (the main spar as part of the entire blade vs. simply supported panel) were essential. It looked as if the local stiffness bending and strength reduction caused by the delamination (for the here simulated cases) in the blade could be compensated by the surrounded blade structure. The main spar as an integrated part of the entire blade structure cannot twist, rotate and strain freely as the panel can. The panels in Branner's study were the more flexibly supported at the panel edges and thus tended to buckle earlier than the spar in the present blade study. Furthermore, the laminated caps in the blade only provide a share to the overall flapwise bending stiffness. Other effects like the distance between the caps, the shear webs and the aerodynamic shell also have a significant contribution to the overall blade bending stiffness, which was neglected in the panel study.

#### 4. Discussion and conclusion

The study showed that modelling buckling driven delamination in wind turbine blades is feasible. The highly discretised sub-modelling approach where a subset of brick elements was connected to a shell element model via suitable couplings constraints, made it possible to predict the effect of delaminations on wind turbine blade structures. Two different subset modelling approaches were applied. One approach was purely based on solid elements and the other included the possibility to simulate delamination growth based on the implementation of cohesive elements.

The cohesive element approach was more comprehensive and provided, due to the possibility of delamination growth simulation, good insights of the delamination process and buckling behaviour. The implementation of cohesive elements was clearly the superior approach compared to the solid element approach because additional information such as the load level for delamination growth onset/propagation could be extracted. Thus, the cohesive element approach made it easier and more precise to evaluate the critical delamination size. The cohesive element approach was the more conservative approach due to the consideration of delamination propagation and its effect on the blade structure.

Beside the different numerical approaches the effect of the delamination on the blade section was studied. The study showed that blade structures with initial delaminations with a width between 30 and 50% of the cap width positioned close to the surface started to grow in load ranges of normal operation conditions and led to local cap opening buckling modes. The local cap opening buckling modes with stable delamination growth (with numerical limitation of maximum delamination growth) caused only little bending stiffness reductions of less than 1.5% compared to the sound structure. Nevertheless, the near-surface local cap buckling modes led to high strains and stresses in the surrounding of the delamination. Therefore, near-surface delamination has to be considered to be critical.

The study showed how critical near-surface delamination in wind turbine blades under design load conditions can be even though only quasi-static loading was applied, the delamination growth was limited in size due to the modelling approach and no ply failure criteria has been considered. In the simulations the delamination growth started at loads of around 50% of the design load. In reality already this normal operation load for local near-surface delaminations would probably be high enough to cause delamination growth due to cyclic loading. At a certain size of the delaminated area and at a corresponding load level local cap opening would occur. High stresses and strains in the sublaminates around the delamination induced by local cap opening would be the consequence. The highly stressed and strained plies would

probably be reduced in their life-time and fatigue failure would occur. Consequently, the adjacent plies have to compensate for the failed plies and would be loaded higher, too. This process would continue until ultimate failure occurs.

Full cap buckling for the here tested blade and delamination configurations did not have any significant effect on the blade response under normal operation conditions. In the simulations the static load exceeded the design load by more than 40% before delamination growth onset or buckling occurred.

The conclusion based on the study is that the load threshold of delamination propagation is highly depending on the location and size of the initial delamination. Delamination induced local cap opening buckling modes have to be considered to be more critical due to an earlier onset of local cap opening buckling compared to full cap buckling modes. This finding is in good agreement with the finding described in Overgaard et al. [9] that moderately sized initial and near-surface delamination will reduce the critical load significantly.

With the hereby presented study the authors came a little closer to the goal of getting to a design criterion for improved and more reliable prediction of delamination induced failure in wind turbine blades.

Interesting future studies would be to investigate how big and in which distance to the outer surface delaminations have to be to become critical and how local delaminations behave under dynamic load conditions.

#### Acknowledgement

The research paper is based upon work supported by the new Danish Centre for Composite Structures and Materials for Wind Turbines (DCCSM), grant no. 09-067212 from the Danish Strategic Research Council. The financial support is greatly appreciated.

#### References

- [1] R.M. Jones, *Mechanics of Composite Materials*, 1975.
- [2] A. Puck, *Festigkeitsanalyse von Faser-Matrix-Laminaten*, Carl Hanser Verlag, Muenchen Wien, 1996.
- [3] H. Schürmann, *Konstruieren mit Faser-Kunststoff-Verbunden*, Vol. 2, Springer-Verlag, Berlin Heidelberg, 2007.
- [4] M.J. Pavier, M.P. Clarke, Experimental techniques for the investigation of the effects of impact damage on carbon fibre composites, *Compos. Sci. Technol.* 55 (1995) 157169.
- [5] S. Abrate, Impact on laminated composite materials, *Appl. Mech. Rev.* 44 (1991) 155–190.
- [6] H.S. Toft, K. Branner, P. Berring, J.D. Sørensen, Defect distribution and reliability assessment of wind turbine blades, *Eng. Struct.* 33 (2011) 171–180. Denmark.
- [7] G.J. Short, F.J. Guild, M.J. Pavier, Delaminations in Flat and Curved Composite Laminates Subjected to Compressive Load, in: *Vols. Composite Structures – Elsevier*, 58, Department of Mechanical Engineering, Bristol – UK, 2002, pp. 249–258.
- [8] L.C.T. Overgaard, E. Lund, Structural collapse of a wind turbine blade. Part A: static test and equivalent single layered models, *Compos. Part A* 41 (2010) 271–283.
- [9] L.C.T. Overgaard, E. Lund, Structural collapse of a wind turbine blade. Part B: progressive interlaminar failure models, *Compos. Part A* 41 (2010) 271–283.
- [10] K. Branner, P. Berring, Compressive strength of thick composite panels, in: *Risø National International Symposium on Material Science*, 2011. Roskilde – Denmark.
- [11] M. Gaotti, M.C. Rizzo, K. Branner, P. Berring, An high order Mixed Interpolation Tensorial Components (MITC) shell element approach for modeling the buckling behavior of delaminated composites, *Compos. Struct.* 108 (2014) 657–666. Genova, Italy.
- [12] B.F. Sørensen, K. Branner, H. Stang, H.M. Jensen, E. Lund, T.K. Jacobsen, K.M. Halling, Improved design of large wind turbine blades of fibre composites (Phase 2) – summary report, Roskilde – Denmark, in: *Risø National Laboratory for Sustainable Energy Risø-R-1526 (EN)*, 2005.
- [13] C. Bak, R.D. Bitsche, A. Yde, T. Kim, M.H. Hansen, F. Zahle, M. Gaunaa, J.P. Blasques, M. Døssing, J.-J. Wedel Heinen, T. Behrens, Light rotor: the 10-MW reference wind turbine, in: *Proceedings of EWEA 2012 – European Wind Energy Conference & Exhibition*, European Wind Energy Association (EWEA), 2012. <http://dtu-10mw-rwt.vindenergi.dtu.dk/>.

- [14] P.D. Soden, M.J. Hinton, A.S. Kaddour, Lamina Properties, Lay-up Configurations and Loading Conditions for a Range of Fibre Reinforced Composite Laminates, in: *Failure Criteria in Fibre Reinforced Polymer Composites: the World-wide Failure Exercise*, 2004, pp. 30–51. Genova, Italy.
- [15] A.T. Travesa, *Simulation of Delamination in Composites under Quasi-static and Fatigue Loading Using Cohesive Zone Models*, University de Girona, Girona – Spain, 2006.
- [16] A. Turon, et al., An Engineering Solution for Using Coarse Meshes in the Simulation of Delamination with Cohesive Zone Models, in: *National Aeronautics and Aerospace Administration*, vol. NASA/TM-2005–213547, Langley Research Center, Hampton, Virginia, United States of America, 2005.
- [17] M. Fiolka, *Theorie und Numerik volumetrischer Schalelemente zur Delaminationsanalyse von Faserverbundlaminaten*, University of Kassel, Kassel – Germany, 2007.
- [18] M.L. Benzeggagh, M. Kenane, Measurement of mixed-mode delamination fracture toughness of unidirectional glass/epoxy composites with mixed-mode bending apparatus, *Compos. Sci. Technol.* 56 (1996) 439449.
- [19] G.J. Marshall, I.H. Turvey, *Buckling and Postbuckling of Composite Plates*, Chapman and Hall, London – UK, 1995.
- [20] P.P. Camanho, C.G. Davila, M.F. Moura, Numerical Simulation of Mixed-Mode Progressive Delamination in Composite Materials, *SAGE – J. Compos. Mater.* 37 (2003).
- [21] Abaqus, Dassault System, in: *Abaqus Analysis Users Manual*, vol. 6.11, 2011.
- [22] J.K. Paik, K. Branner, Y.S. Choo, J. Czujko, Y.S. Fujikubo, J.M. Gordo, G. Parmentier, R. Iaccarino, S. O'Neil, I. Pasqualino, D. Wang, X. Wang, S. Zhang, in: *ISSC Committee III-1 Ultimate Strength 17th International Ship and Offshore Structures Congress*, 16–21 August 2009. Seoul, Korea.
- [23] L.G. Brazier, On the flexure of thin cylindrical shells and other 'thin' sections, *Proc. R. Soc. A, Math. Phys. Eng. Sci.* (September 1927). Published 1.